Correlation strength, orbital-selective incoherence, and local moments formation in the magnetic MAX-phase Mn$_2$GaC

H. J. M. Jönsson [1,*], M. Ekholm [1], I. Leonov [2,3,4], M. Dahlqvist [5], J. Rosen, [5] and I. A. Abrikosov [1,4]

[1]*Theoretical Physics, Department of Physics, Chemistry and Biology (IFM), Linköping University, SE-581 83, Linköping, Sweden*
[2]*M. N. Miheev Institute of Metal Physics, Russian Academy of Sciences, 620108 Yekaterinburg, Russia*
[3]*Ural Federal University, 620002 Yekaterinburg, Russia*
[4]*Materials Modeling and Development Laboratory, National University of Science and Technology "MISiS," Moscow 119049, Russia*
[5]*Materials Design, Department of Physics, Chemistry and Biology (IFM), Linköping University, SE-581 83 Linköping, Sweden*

We perform a theoretical study of the electronic structure and magnetic properties of the prototypical magnetic MAX-phase Mn$_2$GaC with the main focus given to the origin of magnetic interactions in this system. Using the density functional theory+dynamical mean-field theory (DFT+DMFT) method, we explore the effects of electron-electron interactions and magnetic correlations on the electronic properties, magnetic state, and spectral weight coherence of paramagnetic and magnetically ordered phases of Mn$_2$GaC. We also benchmark the DFT-based disordered local moment approach for this system by comparing the obtained electronic and magnetic properties with that of the DFT+DMFT method. Our results reveal a complex magnetic behavior characterized by a near degeneracy of the ferro- and antiferromagnetic configurations of Mn$_2$GaC, implying a high sensitivity of its magnetic state to fine details of the crystal structure and unit-cell volume, consistent with experimental observations. We observe robust local-moment behavior and orbital-selective incoherence of the spectral properties of Mn$_2$GaC, implying the importance of orbital-dependent localization of the Mn 3d states. We find that Mn$_2$GaC can be described in terms of local magnetic moments, which may be modeled by DFT with disordered local moments. However, the magnetic properties are dictated by the proximity to the regime of formation of local magnetic moments, in which the localization is in fact driven by Hund's exchange interaction, and not the Coulomb interaction.

I. INTRODUCTION

MAX-phases are a promising class of functional materials with the generic chemical formula $M_{n+1}AX_n$ and hexagonal crystal structure, which consists of layers of C or N (X) and transition metal (M) atoms, interconnected by layers of the A-group atoms. First discovered in the 1960s [1,2] and later rediscovered in 1996 [3], these materials possess intriguing physical behavior combining the properties typical for ceramics, such as high hardness, and those of metallic systems, e.g., good electrical and thermal conductivity [4]. This combination of physical and mechanical properties, as well as being easily machined [5], makes MAX phases promising for numerous applications, such as thin-film coatings for low friction surfaces, electrical contacts, and heat exchangers [4,5].

In 2013, the first experimental realization of a magnetic MAX-phase of Mn-doped Cr$_2$GeC was presented, synthesized as a heteroepitaxial single crystal thin film with excellent structural quality [6,7]. In 2014, the long-range magnetically ordered Mn$_2$GaC MAX-phase was predicted by *ab initio* band-structure methods and then subsequently synthesized [8]. It was the first magnetic MAX-phase with only Mn atoms as the M-element. Its crystal structure is illustrated in Fig. 1. The layered structure of MAX-phases leads to a variety of possible magnetic structures that offers an intriguing perspective for applications of MAX-phases in spintronics and magnetic refrigeration [9].

Ab initio band-structure calculations, based on density functional theory [10] (DFT) within the local density approximation [11,12] (LDA) or the generalized gradient approximation with the Perdew-Burke-Ernzerhof functional (PBE) [13], propose the existence of robust local magnetic moments in Mn$_2$GaC at low temperatures [14,15], with a ferromagnetic (FM) ground state. In contrast to this, neutron reflectometry in combination with DFT calculations suggests the formation of long-range antiferromagnetic (AFM) order in epitaxial thin films of Mn$_2$GaC [16]. Moreover, the magnetic order was found to be very sensitive to small changes of the lattice volume [15]. A slight expansion of the lattice leads to a transition from the FM to the AFM state with a canted spin structure forming spin spirals with zero net magnetization.
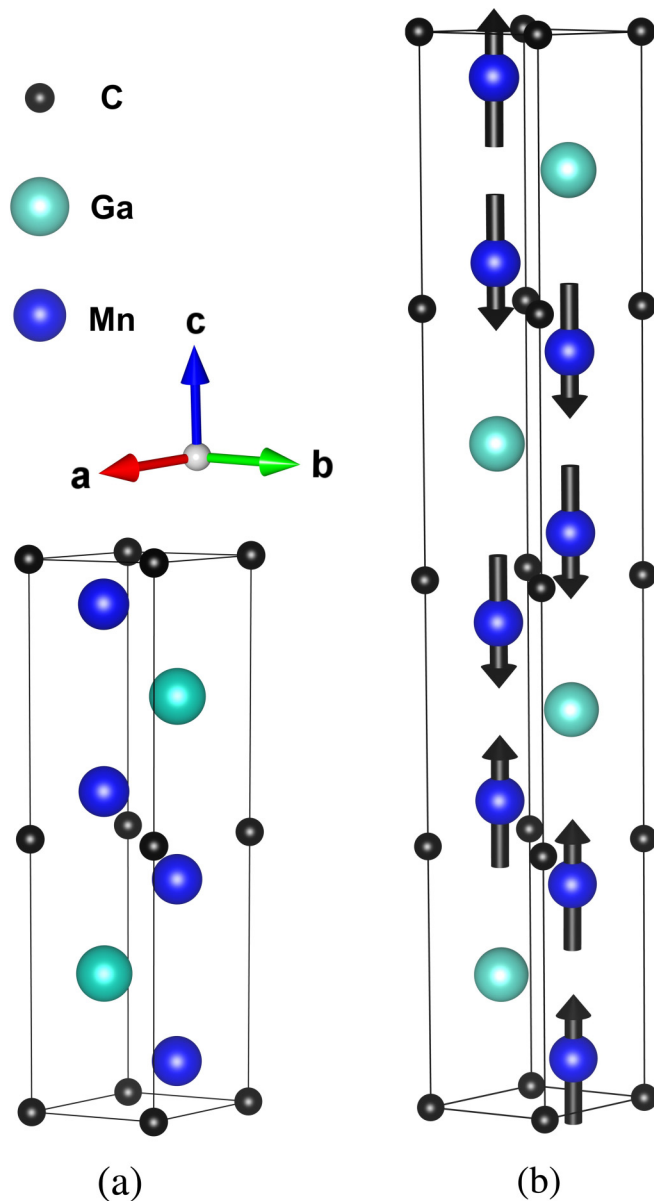
FIG. 1. (a) Crystal structure of Mn_2GaC. The space group is $P6_3/mmc$ with atomic positions: Mn at $4f$ $(\frac{1}{3}, \frac{2}{3}, 0.0821)$, Ga at $2d$ $(\frac{1}{3}, \frac{2}{3}, \frac{3}{4})$, and C at $2a$ $(0, 0, 0)$. (b) An AFM configuration of Mn_2GaC, showing the relative orientation of magnetic moments.

The theoretical calculations were consistent with the experimentally observed high sensitivity of the magnetic state of Mn_2GaC on temperature around room temperature [15].

The complicated behavior of the ordered magnetic structure of Mn_2GaC has also been observed in experiments [16,17]. In particular, above ~507 K there appears to be a transition from a collinear AFM to a paramagnetic (PM) state, while below 214 K there is a transition from a collinear AFM to a canted AFM state. In contrast to previously suggested local moment behavior, experimental studies of the MAX-phase $(Cr,Mn)_2GaC$ with up to 25% Mn report the FM state due to itinerant electrons, ruling out localized magnetic moments residing on the Mn sites [18]. This raises a question about magnetic moments in Mn_2GaC in terms of itinerant or

localized electronic states, which poses a challenge for an accurate microscopic description of the electronic and magnetic properties of Mn_2GaC.

In this work, we explore the electronic structure and magnetic properties of Mn_2GaC using the DFT+dynamical mean-field theory (DFT+DMFT) approach for strongly correlated systems [19–21]. By using the DFT+DMFT approach, it becomes possible to proceed beyond a static mean-field treatment of the electron-electron interactions in DFT to capture correlated electron phenomena such as quasiparticle behavior, orbital-selective band mass renormalizations, and coherence-incoherence crossover of the spectral weight. It also enables us to consider temperature-induced (local) quantum fluctuations, and to explain the Mott transition [19,20,22–34]. Our results suggest that Mn_2GaC is a correlated metal sitting near the regime of formation of local magnetic moments, in which localization is driven by the on-site Hund's exchange coupling J (in contrast to the Hubbard repulsion U value).

II. COMPUTATIONAL DETAILS

We employ the state-of-the-art fully self-consistent in charge density DFT+DMFT method [19,20] to examine the electronic structure and magnetic properties of paramagnetic and magnetically ordered states of Mn_2GaC. In our DFT+DMFT calculations, we use two independent DFT+DMFT implementations. The first is provided in the Toolbox for research in interacting quantum systems (TRIQS) package for DMFT, which is interfaced with the all-electron WIEN2K DFT code [21,35–39]. We used LDA and set $R_{MT}K_{max} = 8.0$. In DFT+DMFT calculations, we consider the Mn $3d$ valence states as correlated orbitals by constructing a basis set of atomic-centered Wannier functions within the energy window $[-7.8, 6.4]$ eV (Fermi energy $E_F = 0$) [38,40,41]. We use the continuous-time hybridization expansion quantum Monte Carlo algorithm within the full rotationally invariant form in order to solve the realistic many-body problem in DMFT [42–47], as implemented in the CTHYB package [48].

In the second case, we use DFT+DMFT implemented within a plane-wave pseudopotential formalism [28–31] in DFT [49], combined with the continuous-time hybridization expansion (segment) quantum Monte Carlo algorithm in DMFT [19,20,47]. In this approach, the Coulomb interaction is treated in the density-density approximation, neglecting by spin-flip and pair-hopping terms in the multiorbital Hubbard Hamiltonian. We use the generalized gradient approximation with the PBE functional in DFT [13]. In our DFT+DMFT calculations, we explicitly include the Mn $3d$, Ga $4s$ and $4p$, and C $2p$ valence states by constructing a basis set of atomic-centered Wannier functions within the energy window spanned by these bands [40,41]. This allows us to take into account charge transfer between the partially occupied Mn $3d$, Ga $4s$ and $4p$, and C $2p$ valence states, accompanied by the strong on-site Coulomb correlations of the Mn $3d$ electrons. The DFT+DMFT calculations are performed with full self-consistency over the charge density.

Using both DFT+DMFT approaches, we compute the electronic structure, magnetic properties, quasiparticle mass renormalizations m^*/m, and spin-spin correlation function

$\chi(\tau)$ of the PM, FM, and AFM states of Mn_2GaC as shown in Fig. 1. We note that in our spin-polarized DFT+DMFT calculations, the nonmagnetic DFT was employed (exchange splitting due to magnetism appears in DMFT). We take $U = 3.8$ eV for the average Hubbard interaction, as estimated previously using the constrained random phase approximation [50], and Hund's exchange coupling $J = 0.95$ eV. In addition, we explore the effects of correlation strength on the electronic and magnetic properties of Mn_2GaC taking the different values of the Coulomb repulsion and Hund's exchange couplings $U = 5.3$ and 6.9 eV, and $J = 0.5$ eV, respectively [51–54].

To analyze the degree of localization of the Mn $3d$ electrons of the PM, FM, and AFM Mn_2GaC, we compute the local spin-spin correlation function $\chi(\tau) = \langle \hat{m}_z(\tau)\hat{m}_z(0)\rangle$ within DMFT, where $\hat{m}_z(\tau)$ is the instantaneous magnetization on the Mn $3d$ site at the imaginary time τ (the latter denotes an imaginary-time evolution ranging from 0 to $\beta = 1/k_B T$ in the path integral formalism) [19,20]. In both DFT+DMFT calculations, the fully localized double-counting correction evaluated from the self-consistently determined local occupations was used. The spin-orbit coupling is neglected in our calculations. To obtain the self-energy on the real axis, we employ the maximum entropy method, as implemented in the MAXENT package [55] and Padé approximants.

In Fig. 1(a) we display the nonmagnetic two-formula-units cell (contains eight atoms) of Mn_2GaC with a lattice volume of 40.87 Å^3/f.u. and $c/a = 4.3$, used in the DFT+DMFT calculations (the corresponding lattice parameters are evaluated from optimization of the unit-cell shape within nonmagnetic DFT). In addition, we compute the electronic and magnetic properties of PM Mn_2GaC with DFT-PBE for magnetically disordered supercells of Mn_2GaC using the projector-augmented waves technique [56], as implemented in the Vienna *ab-initio* simulation package (VASP) [57,58]. To this end, we set up a 128-atom supercell consisting of $4 \times 4 \times 1$ unit cells. To model the PM state, we distributed the up/down Mn magnetic moments according to the special quasirandom structure (SQS) technique [59,60]. We minimize the short-range-order parameter [61] $\alpha_i = 1 - \frac{P_i(\uparrow|\downarrow)}{c^\downarrow}$, where $P_i(\uparrow|\downarrow)$ is the average conditional probability of finding a spin-down Mn atom in the ith coordination shell of a spin-up atom on the Mn sublattice; $c^\downarrow = 0.5$ is the concentration of spin-down atoms on the sublattice. After self-consistency, one of the 64 Mn magnetic moments had flipped. Nevertheless, the absolute value of the short-range order parameters was below 0.08 for the first eight nearest-neighbor shells. In these calculations, we used a $5 \times 5 \times 5$ **k**-point mesh and a plane-wave cutoff 400 eV. The unit-cell volume was taken to be 44.66 Å^3/f.u. and $c/a = 4.29$ as obtained from structural optimization of Mn_2GaC within static DFT-SQS (for details, see Ref. [15]).

III. RESULTS

A. FM and AFM long-range-ordered magnetic states

We start by computing the electronic structure and magnetic properties of the FM and AFM phases of Mn_2GaC at a temperature $T = 193$ K using the spin-polarized

TABLE I. Long-range-ordered $\langle \hat{m}_z \rangle$, fluctuating M_{loc}, and instantaneous $\sqrt{\langle \hat{m}_z^2 \rangle}$ magnetic moments of Mn ions of the FM, AFM, and PM phases of Mn_2GaC as obtained by DFT+DMFT at different temperatures. The Hubbard interaction $U = 3.8$ eV. In the DFT+DMFT results at $T = 116$ K, Hund's exchange is taken to be $J = 0.5$ eV, while at $T = 193$ and 1160 K, $J = 0.95$ (see the text).

	116 K		193 K		1160 K
	AFM	PM	FM	AFM	PM
$\langle \hat{m}_z \rangle$	0.12	0	1.70	1.73	0
M_{loc}	0.31	0.3	1.72	1.76	1.4
$\sqrt{\langle \hat{m}_z^2 \rangle}$	1.8	1.81	2.2	2.2	2.3

DFT+DMFT method with $U = 3.8$ eV and $J = 0.95$ eV. We note that both DFT+DMFT schemes discussed above give nearly identical results. In Fig. 2 we display our DFT+DMFT results for the Mn $3d$, Ga $4p$, and C $2p$ spectral functions of Mn_2GaC. Our results for the **k**-resolved spectral functions $A(\mathbf{k}, \omega) = -\frac{1}{\pi} \mathrm{Tr} G(\mathbf{k}, \omega)$ of the FM and AFM phases of Mn_2GaC are shown in Figs. 3 and 4.

We find a metallic solution with a long-range magnetic ordering of the Mn ions. The Mn $3d$ states are strongly hybridized with the C $2p$ and Ga $4p$ states and form a broadband of about 8 eV bandwidth located at the Fermi level. The occupied C $2p$ and Ga $4p$ states appear in between about -8 to -4 eV and near -4 eV below E_F, respectively. The unoccupied C $2p$ and Ga $4p$ bands sit above 2 eV. The spectral functions of FM and AFM Mn_2GaC show a pronounced $\sim$1–2 eV splitting of the Mn $3d$ spin-up and spin-down states due to the magnetic exchange (see Fig. 2).

Our results for the self-energy show a typical Fermi-liquid-like behavior, though with a notable damping of quasiparticles of the Mn t_2 (a_{1g} and e_g^π) orbitals in the AFM state [$\mathrm{Im}[\Sigma(0^+)] \sim 0.01$–$0.03$ eV]. The latter is seen as (orbital-selective) incoherence of the **k**-resolved spectral weight of the Mn $3d$ states near the Fermi level in Mn_2GaC (see Figs. 3 and 4), implying the importance of electronic correlations [32–34,62–66]. Moreover, we evaluate the quasiparticle mass enhancement $m^*/m = 1 - \partial \mathrm{Im}\Sigma(\omega)/\partial\omega|_{\omega=0}$ using extrapolation of the self-energy $\Sigma(\omega)$ to $\omega = 0$ eV, which gives a quantitative measure of the correlation strength. For the long-range FM and AFM ordered states, we obtain a moderately correlated metal with $m^*/m \sim 1.4$ and 1.6, respectively, with a weak orbital-dependence of m^*/m. In fact, the electronic band structure obtained by DFT+DMFT closely follows the spin-polarized DFT results, with a notable bandwidth renormalization and significant broadening (incoherence) of the spectral weight caused by correlation effects.

The calculated long-range ordered magnetic moments for the FM and AFM states (at 193 K), $\sim$1.70μ_B and 1.73μ_B per Mn ion, respectively, are comparable to those found within spin-polarized DFT (PBE) for the theoretical equilibrium volume, 1.59μ_B and 1.83μ_B [15] (see Table I). At the same time, the instantaneous magnetic moment $\sqrt{\langle \hat{m}_z^2 \rangle}$ is higher, $\sim$2.5μ_B, implying the presence of significant (local) spin fluctuations. To quantify the robustness of magnetic moments of the Mn $3d$ states with respect to quantum fluctuations, we compute the local spin-spin correlation function
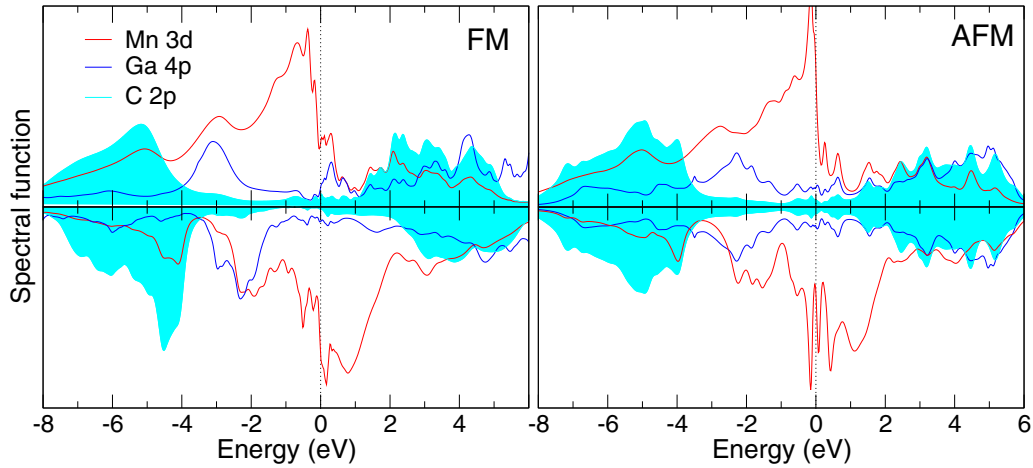
FIG. 2. Mn 3d, Ga 4p, and C 2p spectral functions of the FM and AFM phases of Mn$_2$GaC obtained within the spin-polarized DFT+DMFT calculations at $T = 290$ K.

$\chi(\tau) = \langle \hat{m}_z(\tau) \hat{m}_z(0) \rangle$ within DMFT. Our DFT+DMFT results for $\chi(\tau)$ are summarized in Fig. 5. Our analysis of the local spin susceptibility suggests the proximity of Mn 3d moments to localization. In particular, while $\chi(\tau)$ is seen to slowly decay with the imaginary time at small τ (mainly for $\tau/\beta < 0.05$), it is significant and nearly constant for $\tau \simeq \beta/2$, $\sim 3.0 \mu_B^2$, which implies the robustness of local magnetic moments in Mn$_2$GaC. Moreover, the calculated fluctuating local moments $M_{loc} = [T \int_0^{1/T} d\tau \langle \hat{m}_z(\tau) \hat{m}_z(0) \rangle]^{1/2}$ are $\sim 1.72 \mu_B$ and 1.76μ_B for the FM and AFM states, respectively. The

latter are compatible with the long-range magnetic moment of ~ 1.70–$1.73 \mu_B$ per Mn ion in FM and AFM Mn$_2$GaC.

Our DFT+DMFT total-energy calculations (with $U = 3.8$ eV and $J = 0.95$ eV) suggest a near degeneracy of the FM and AFM states of Mn$_2$GaC. In particular, we find that at 193 K the AFM state is energetically favorable, with a small total energy difference between the FM and AFM state of ~ 4 meV/f.u., whereas at 293 K it differs by -5 meV/f.u., with the FM state being most stable. This behavior suggests a high sensitivity of the magnetic state of Mn$_2$GaC, e.g., to fine
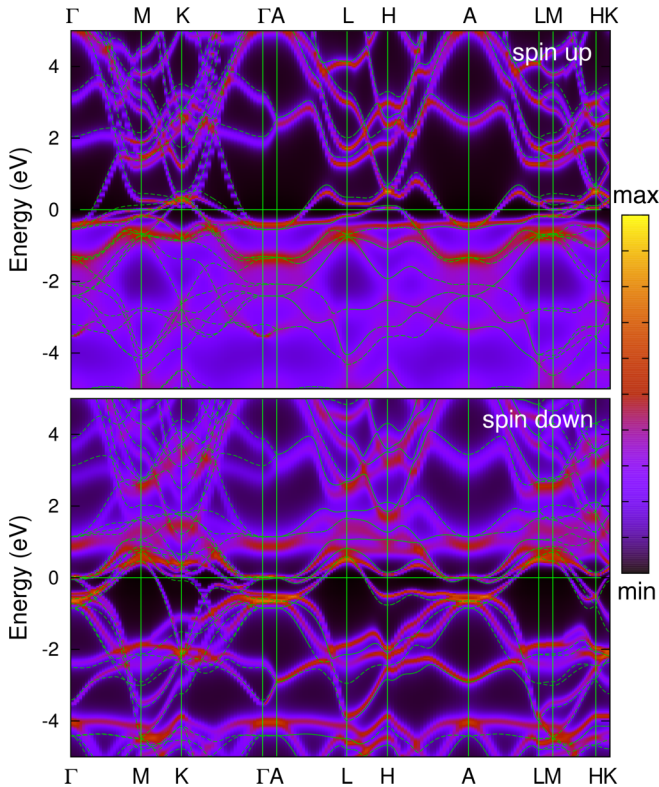

FIG. 3. **k**-resolved spectral function of FM Mn$_2$GaC calculated by DFT+DMFT at $T = 290$ K in comparison to the spin-polarized DFT results (shown in green).
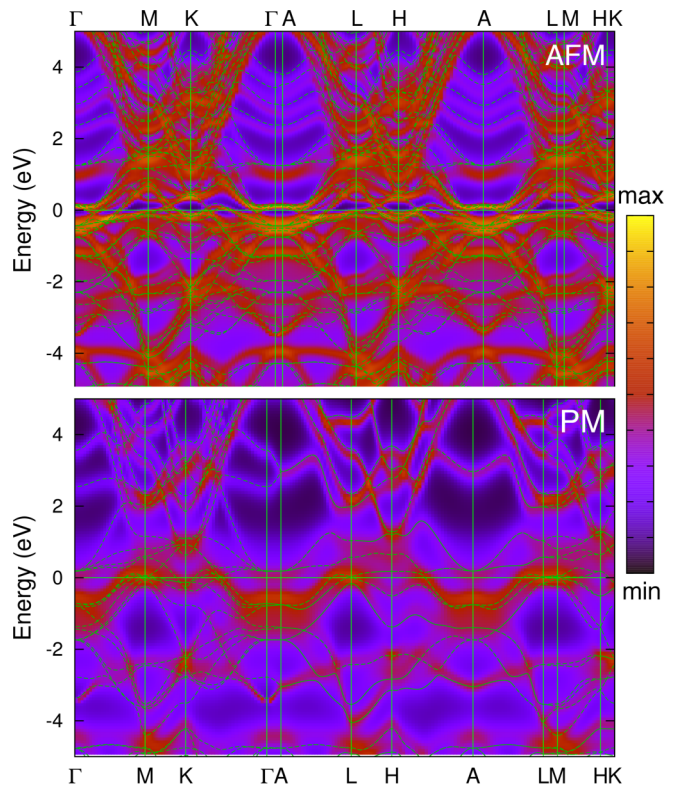

FIG. 4. **k**-resolved spectral function of the AFM and PM phases of Mn$_2$GaC calculated by DFT+DMFT in comparison to the "bare" Kohn-Sham band structure obtained within DFT (shown in green).
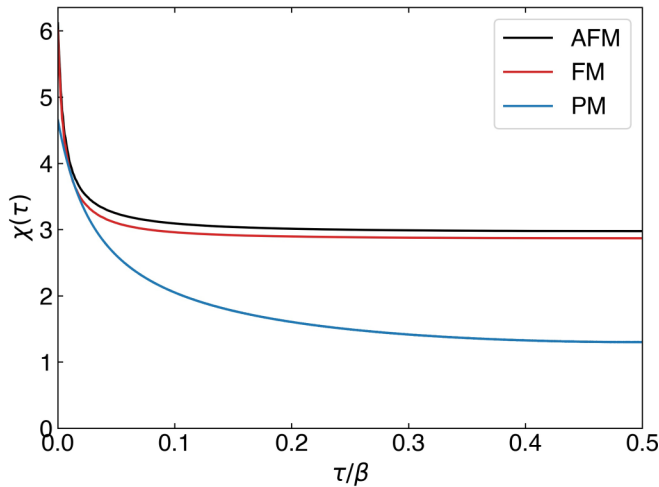
FIG. 5. Local spin-spin correlation function $\chi(\tau) = \langle \hat{m}_z(\tau) \hat{m}_z(0) \rangle$ calculated by DFT+DMFT (with $U = 3.8$ eV and $J = 0.95$ eV) as a function of the imaginary time τ. Our DFT+DMFT results for the FM and AFM phases at $T \sim 193$ K ($\beta = 60$ eV^{-1}) and the PM phase at $T \sim 1160$ K ($\beta = 10$ eV^{-1}) are shown.

details of its crystal structure, lattice volume, and temperature, in agreement with experimental observations. At the same time, the PM state is found to be highly energetically unfavorable, with a total energy difference of $\sim$95 meV/f.u., suggesting strong magnetic exchange interactions in Mn$_2$GaC.

Moreover, we observe that the magnetic properties of Mn$_2$GaC depend very sensitively on the particular choice of Hund's exchange coupling J. In fact, for a smaller value $J = 0.5$ eV (and the same Hubbard interaction $U = 3.8$ eV), both the FM and AFM states are found to be unstable and collapse to the PM state at room temperature. At $\sim$116 K for AFM Mn$_2$GaC, we find long-range magnetic ordering with a weak static magnetic moment of $\sim 0.12\mu_B$ per Mn ion. We note that at $\sim$116 K the FM phase is unstable and collapses in the PM state. The calculated instantaneous local moments are significantly smaller, $\sim 1.8\mu_B$, than those for $J = 0.95$ eV. In addition to this, our DFT+DMFT calculations with $U = 3.8$ eV and $J = 0.5$ eV of the local spin susceptibility $\chi(\tau)$ give a typical itinerant moment behavior, with $\chi(\tau)$ quickly decaying to zero with the imaginary time τ. Our result for the fluctuating moment is $\sim 0.3\mu_B$ (at $\sim$116 K).

B. Paramagnetic phase

Next, we compute the electronic structure and magnetic state of the PM phase of Mn$_2$GaC at a high electronic temperature $T \sim 1160$ K (well above the experimental magnetic ordering temperature of $\sim$507 K) using the DFT+DMFT method with $U = 3.8$ eV and $J = 0.95$ eV. In Fig. 4 (bottom panel) we display our results for the **k**-resolved spectral function of PM Mn$_2$GaC in comparison with the "bare" Kohn-Sham band structure, calculated within nonmagnetic DFT. Our results for the orbitally resolved Mn 3d, Ga 4p, and C 2p spectral functions of PM Mn$_2$GaC are shown in Fig. 6.
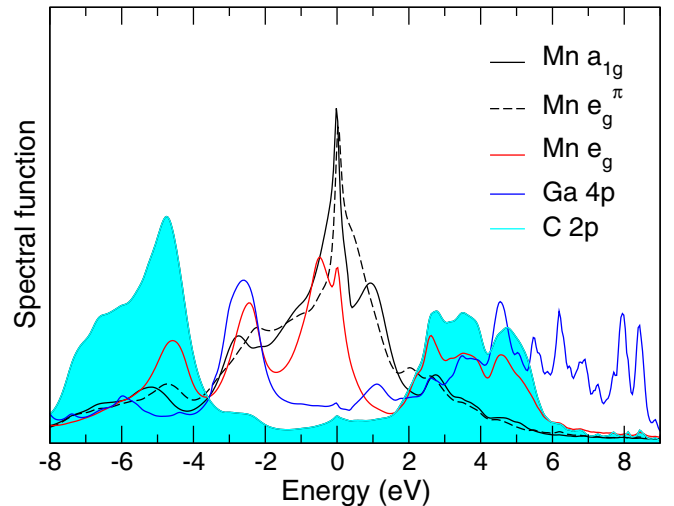

FIG. 6. Orbitally resolved Mn 3d, Ga 4p, and C 2p spectral functions of PM Mn$_2$GaC obtained by DFT+DMFT.

We obtain a strongly correlated metal with a pronounced quasiparticle peak at the Fermi level due to the Mn a_{1g} and e_g^π states. The Mn e_g^σ states are seen to strongly hybridize with the Ga 4p and C 2p states and are of about 10 eV bandwidth. In contrast, the Mn t_2 bandwidth is more narrow at $\sim$6 eV, suggesting the importance of orbital-selective correlations. Mn$_2$GaC is characterized by a Fermi-liquid-like behavior of the self-energy and large damping (finite lifetime) of quasiparticles originating from the Mn t_2 states and Im[$\Sigma(0^+)$] $\sim$ 0.34 eV in the PM state at 290 K, respectively (see Fig. 7). For the Mn e_g^σ states it is weaker, at $\sim$0.14 eV. The latter is consistent with significant (orbital-dependent) incoherence of the spectral weight of the Mn 3d states near the Fermi level [see Fig. 4 (bottom panel)], implying the importance of electronic correlations [32–34,62–66]. This behavior persists even at relatively low temperature of $\sim$193 K (in the PM state). Moreover, our analysis of the orbitally resolved quasiparticle mass renormalizations yields $m^*/m \sim 2.6$ and 1.6 for the Mn t_2 (a_{1g} and e_g^π) and e_g^σ states, respectively, implying orbital selectivity of correlation effects in Mn$_2$GaC. The latter agrees well with sufficiently different bandwidth of the Mn t_2 and e_g^σ states, as well as with orbital-selective incoherence of the Mn 3d states. Our results for the instantaneous magnetic moment of the Mn ions is $\sim 2.3\mu_B$. This value is larger than the long-range-ordered magnetic moment obtained by DFT+DMFT for the FM and AFM phases of Mn$_2$GaC at $T \sim 193$ K, $\sim 1.7\ \mu_B$ per Mn ion, due to temperature-induced quantum fluctuations.

In addition to this, our results for the local spin susceptibility $\chi(\tau)$ (with $U = 3.8$ eV and $J = 0.95$ eV) show the presence of local moment behavior in PM Mn$_2$GaC. $\chi(\tau)$ shows a slow decay with the imaginary time τ to a nearly flat region with $\chi \simeq 1.4\mu_B^2$ near $\tau \simeq \beta/2$, implying the robustness of local magnetic moments in the PM phase. Moreover, the calculated fluctuating moment M_{loc} is large, $\sim 1.4\mu_B$, consistent with the regime of formation of local magnetic moments. Our results reveal a remarkable orbital-selective renormalization of the Mn 3d bands in PM Mn$_2$GaC, which suggests orbital-dependent localization of the Mn 3d states.
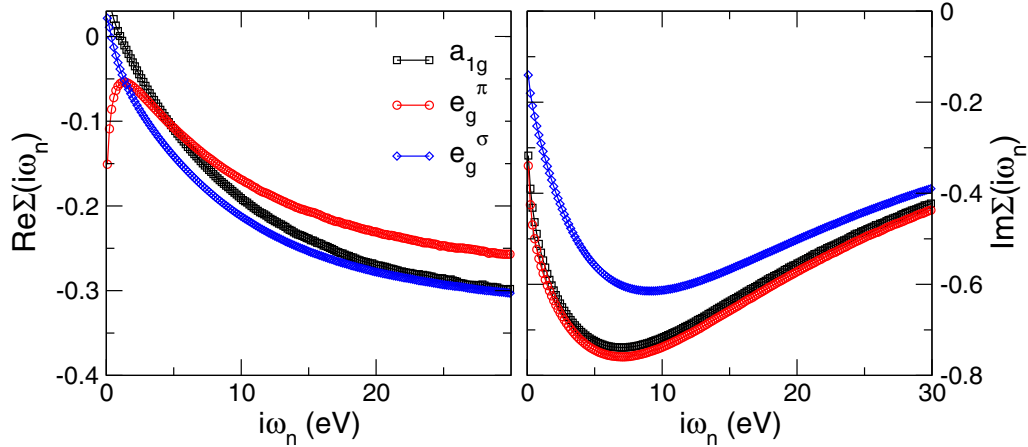
FIG. 7. Orbitally resolved Mn $3d$ self-energy on Matsubara contour $\Sigma(i\omega_n)$ of PM Mn_2GaC evaluated by DFT+DMFT.

We notice a remarkable *increase* of local moments (both instantaneous and fluctuating) in the low-temperature FM and AFM Mn_2GaC, suggesting an *enhancement* of localization of the Mn $3d$ states in the FM and AFM phases of Mn_2GaC. On the other hand, this behavior is accompanied by a sizable decrease of the quasiparticle mass renormalizations, suggesting the importance of orbital-selective damping of quasiparticle coherence, i.e., an enhancement of the strength of electronic correlations.

Interestingly, in contrast to a sharp dependence on Hund's exchange J, we observe a rather weak change of the electronic structure and magnetic properties (e.g., local moments) upon a large variation of the Hubbard U value from 3.8 to 5.3 and 6.9 eV. In particular, the instantaneous moments increase from $2.3\mu_B$ to $2.5\mu_B$, i.e., only by less than 9% upon a change of the Hubbard U from 3.8 to 6.9 eV (with $J = 0.95$ eV). This anomalous dependence of the electronic and magnetic properties of Mn_2GaC on Hund's coupling J, with a rather weak dependence on the Hubbard U, is reminiscent of that in Hund's metals [67–76]. We conclude that the magnetic properties of Mn_2GaC are dictated by its proximity to the regime of formation of local magnetic moments, in which localization is driven by Hund's exchange coupling J. This implies the crucial importance of (orbital-dependent) correlation effects for understanding the electronic and magnetic properties of Mn_2GaC.

To better establish the relation between our advanced DFT+DMFT calculations [77] with earlier simulations of Mn_2GaC carried out with DFT, we have performed DFT calculations of the magnetic properties of PM Mn_2GaC within the static disordered local moment (DLM) picture. In this approach, the quantum PM state is approximated by disordered local magnetic moments distributed over the Mn sites in the supercell of Mn_2GaC consisting of $4 \times 4 \times 1$ unit cells to mimic complete magnetic disorder in the thermodynamic limit [60], although neglecting quantum fluctuations. In Fig. 8 we display a histogram over the magnitudes of local magnetic moments of the Mn ions. It has a mean value of $\sim 1.7\mu_B$, compatible to the fluctuating local magnetic moments obtained by DFT+DMFT, with a significant portion of magnetic moments deviating from the mean value. This indicates a sensitivity of

magnetic moments to the local environment, which is usually seen in itinerant electron magnets [78].

In Fig. 9 we compare the density of states (DOS) obtained within DFT with the **k**-integrated spectral function from DFT+DMFT. In addition to DLM, we also include nonmagnetic DFT (PBE) calculations. We note that in the DFT-DLM results, the main characteristic features of the nonmagnetic DOS are still present, and the electronic structure of all local environments adds up to a very similar DOS to that in the nonmagnetic DFT description. This is in line with the fact that the DFT+DMFT calculations retain the large quasiparticle peak due to the Mn $3d$ states near the Fermi energy that is seen in the DFT results, although it is significantly renormalized due to correlation effects.

IV. DISCUSSION

The electronic structure and magnetic properties of MAX-phases have received much attention in condensed-matter physics during the past decade. Nonetheless, the nature
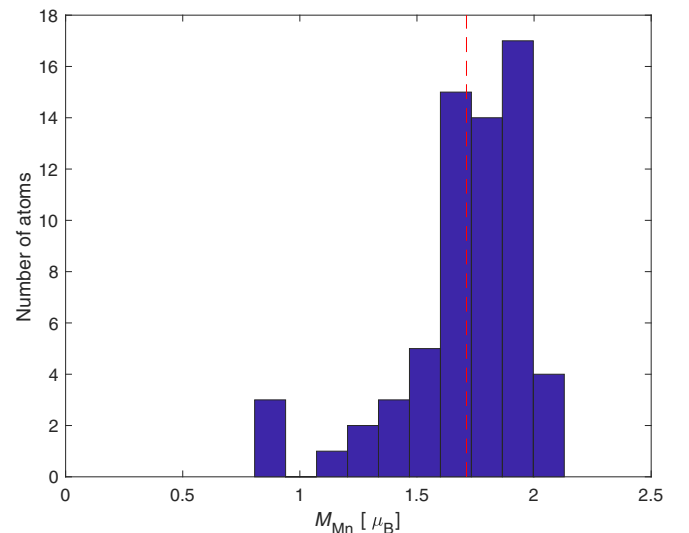

FIG. 8. Distribution of Mn magnetic moments obtained from supercell DFT-DLM calculations with PBE.
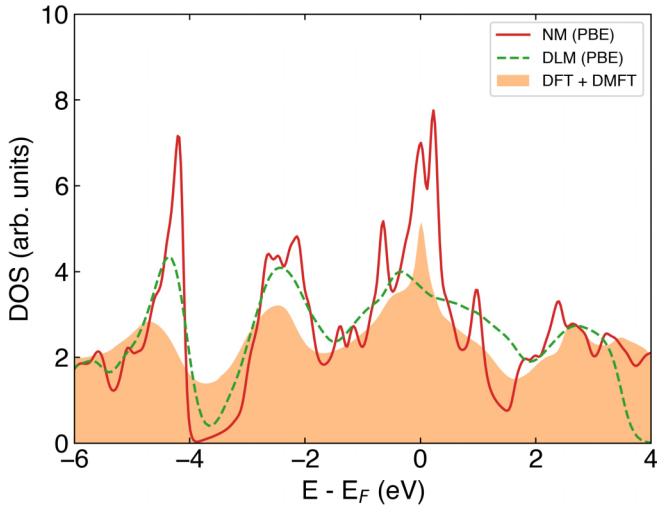
FIG. 9. Density of states of Mn_2GaC obtained within nonmagnetic PBE (solid red line), disordered local moments within the PBE approximation (dashed green line), and the DFT+DMFT total spectral function (solid orange field). The energy scale is relative to the Fermi energy, E_F.

of their magnetic interactions, e.g., the origin of magnetic moments of the prototypical magnetic MAX-phase compound Mn_2GaC, has remained controversial. In our study, we compute the electronic structure and magnetic properties of the PM, FM, and AFM phases of Mn_2GaC using the DFT+DMFT and DFT-DLM electronic structure methods. While DFT-DLM gives a static configurational treatment of the PM state, by using DFT+DMFT it becomes possible to treat dynamical quantum fluctuation effects at finite temperatures and to study local moment formation in Mn_2GaC.

For the PM phase using DFT+DMFT, we find a correlated metal with a Fermi-liquid-like behavior of the self-energy exhibiting a large orbital-selective quasiparticle damping (for the Mn t_2 and e_g^σ states $Im[\Sigma(0^+)] \sim 0.34$ and ~ 0.14 eV in the PM state at 290 K, respectively) and remarkable orbital-selective renormalization of the Mn $3d$ bands. It leads to a sufficiently strong orbital-selective incoherence of the spectral weight of the Mn $3d$ states near the Fermi level, implying the importance of electronic correlation effects. Our DFT+DMFT results reveal a complex magnetic behavior of Mn_2GaC with strongly competing FM and AFM states at low temperatures. This suggests a high sensitivity of the magnetic state of Mn_2GaC to fine details of its crystal structure, lattice volume, pressure, etc., in agreement with recent experiments. Moreover, this suggests the possible importance of structural optimization of the atomic positions and unit-cell shape of Mn_2GaC within DFT+DMFT, which remains a great challenge for the future [79–83]. While the ordered magnetic moments obtained by DFT+DMFT for the FM and AFM states ($\sim 1.7 \mu_B$) are compatible with those found with spin-polarized DFT, the instantaneous magnetic moment is sufficiently higher ($\sim 2.5 \mu_B$), implying the presence of significant (local) spin fluctuations. Our analysis of the local spin susceptibility suggests the proximity of the Mn $3d$ moments to localization, consistent with a large quasiparticle damping of the Mn t_2 orbitals in the PM state. At the same time, the quasiparticle band renormalization of the Mn $3d$ states in

the long-range magnetically ordered FM and AFM phases is found to be relatively weak, about 1.5.

We observe that the magnetic properties of Mn_2GaC depend very sensitively on the choice of Hund's exchange coupling, with a typical itinerant magnetism and coherent quasiparticle behavior for $J = 0.5$ eV and robust local moments behavior for $J = 0.95$ eV. Moreover, DFT+DMFT calculations with $J = 0.5$ eV give a sharp suppression of the magnetic ordering temperature to ~ 116 K, resulting in a weak ordered magnetic moment of $\sim 0.12 \mu_B$ per Mn ion (at ~ 116 K), in contradiction with experiment. Most importantly, our calculations show that the magnetic properties of Mn_2GaC are dictated by its proximity to the regime of formation of local magnetic moments, in which localization is driven by Hund's exchange coupling J. We observe that the quantum dynamics of the system is driven by Hund's exchange instead of the Coulomb repulsion, suggesting that Mn_2GaC is a representative of Hund's metals. This results in a remarkable orbital-dependent incoherence of the spectral weight of PM Mn_2GaC, which is different from the DFT-based DLM results.

Our DFT+DMFT calculations suggest the robustness of local magnetic moments of the Mn ions in this compound. This explains why the previous DFT calculations give reliable results for the long-range-ordered magnetic state of Ma_2GaC. The robust local moment behavior seems to validate the use of a static configurational DFT-DLM treatment of the PM state of Mn_2GaC, while the magnitude of the localized magnetic moments is found to be affected by temperature-induced excitations. Moreover, the DFT-based description of the high-temperature PM state of Mn_2GaC in the framework of the static mean-field DLM picture leads to a mean magnetic moment of $\sim 1.7 \mu_B$, compatible with the fluctuating local magnetic moments obtained by DFT+DMFT. At the same time, the DFT+DMFT calculations suggest the presence of significant (local) spin fluctuations in Mn_2GaC. This effect seems to be partly captured in our DFT-DLM calculations where a significant portion of the magnetic moments deviates from the mean value.

V. SUMMARY AND CONCLUSIONS

In conclusion, we performed a theoretical study of the electronic structure and magnetic properties of the PM, FM, and AFM states of the prototypical MAX-phase Mn_2GaC using the DFT+DMFT and DFT-DLM methods. Our DFT+DMFT results show robust local-moment behavior and orbital-selective incoherence of the spectral properties of Mn_2GaC, which imply the importance of orbital-dependent localization of the Mn $3d$ states. This suggests the crucial importance of (orbital-dependent) correlation effects for understanding the electronic and magnetic properties of Mn_2GaC.

Our calculations reveal a complex magnetic behavior of Mn_2GaC with strongly competing FM and AFM states at low temperatures. This suggests a high sensitivity of the magnetic state of Mn_2GaC to fine details of its crystal structure, lattice volume, pressure, etc., in agreement with recent experiments. This is in agreement with the results of the previous DFT calculations of the long-range magnetically ordered states of Mn_2GaC, while the robust local moment behavior seems to validate the use of a static configurational DFT-DLM treatment of the PM state of Mn_2GaC.

Most importantly, our calculations show that the magnetic properties of Mn$_2$GaC are dictated by its proximity to the regime of formation of local magnetic moments, in which localization is driven by Hund's exchange coupling J. We observe that the quantum dynamics of the system is driven by Hund's exchange instead of the Coulomb repulsion, suggesting that Mn$_2$GaC is a representative of Hund's metals. Our results may have important implications for the theoretical and experimental understanding of the magnetic properties of MAX phases. We believe that this topic deserves further detailed theoretical and experimental considerations.

[1] H. Rohde and H. Kudielka, Z. Kristall. **114**, 447 (1960).

[2] V. H. Nowotny, Prog. Solid State Chem. **5**, 27 (1971).

[3] M. W. Barsoum and T. El-Raghy, J. Am. Ceram. Soc. **79**, 1953 (1996).

[4] P. Eklund, M. Beckers, U. Jansson, H. Högberg, and L. Hultman, Thin Solid Films **518**, 1851 (2010).

[5] M. W. Barsoum and M. Radovic, Annu. Rev. Mater. Res. **41**, 195 (2011),.

[6] A. S. Ingason, A. Mockute, M. Dahlqvist, F. Magnus, S. Olafsson, U. B. Arnalds, B. Alling, I. A. Abrikosov, B. Hjörvarsson, P. O. A. Persson, and J. Rosen, Phys. Rev. Lett. **110**, 195502 (2013).

[7] S. Lin, P. Tong, B. S. Wang, Y. N. Huang, W. J. Lu, D. F. Shao, B. C. Zhao, W. H. Song, and Y. P. Sun, J. Appl. Phys. **113**, 053502 (2013).

[8] A. Ingason, A. Petruhins, M. Dahlqvist, F. Magnus, A. Mockute, B. Alling, L. Hultman, I. Abrikosov, P. Persson, and J. Rosen, Mater. Res. Lett. **2**, 89 (2014).

[9] A. S. Ingason, M. Dahlqvist, and J. Rosen, J. Phys.: Condens. Matter **28**, 433003 (2016).

[10] P. Hohenberg and W. Kohn, Phys. Rev. **136**, B864 (1964).

[11] W. Kohn and L. J. Sham, Phys. Rev. **140**, A1133 (1965).

[12] J. P. Perdew and Y. Wang, Phys. Rev. B **45**, 13244 (1992).

[13] J. P. Perdew, K. Burke, and M. Ernzerhof, Phys. Rev. Lett. **77**, 3865 (1996).

[14] A. Thore, M. Dahlqvist, B. Alling, and J. Rosen, Phys. Rev. B **93**, 054432 (2016).

[15] M. Dahlqvist, A. S. Ingason, B. Alling, F. Magnus, A. Thore, A. Petruhins, A. Mockute, U. B. Arnalds, M. Sahlberg, B. Hjörvarsson, I. A. Abrikosov, and J. Rosen, Phys. Rev. B **93**, 014410 (2016).

[16] A. S. Ingason, G. K. Pálsson, M. Dahlqvist, and J. Rosen, Phys. Rev. B **94**, 024416 (2016).

[17] I. P. Novoselova, A. Petruhins, U. Wiedwald, Á. S. Ingason, T. Hase, F. Magnus, V. Kapaklis, J. Palisaitis, M. Spasova, M. Farle, J. Rosen, and R. Salikhov, Sci. Rep. **8**, 2637 (2018).

[18] Z. Liu, T. Waki, Y. Tabata, and H. Nakamura, Phys. Rev. B **89**, 054435 (2014).

[19] A. Georges, G. Kotliar, W. Krauth, and M. J. Rozenberg, Rev. Mod. Phys. **68**, 13 (1996).

[20] G. Kotliar, S. Y. Savrasov, K. Haule, V. S. Oudovenko, O. Parcollet, and C. A. Marianetti, Rev. Mod. Phys. **78**, 865 (2006).

[21] M. Aichhorn, L. Pourovskii, V. Vildosola, M. Ferrero, O. Parcollet, T. Miyake, A. Georges, and S. Biermann, Phys. Rev. B **80**, 085101 (2009).

[22] R. M. Martin, L. Reining, and D. M. Ceperley, *Interacting Electrons: Theory and Computational Approaches* (Cambridge University Press, Cambridge, 2016).

[23] A. A. Katanin, A. I. Poteryaev, A. V. Efremov, A. O. Shorikov, S. L. Skornyakov, M. A. Korotin, and V. I. Anisimov, Phys. Rev. B **81**, 045117 (2010).

[24] I. Leonov, A. I. Poteryaev, V. I. Anisimov, and D. Vollhardt, Phys. Rev. Lett. **106**, 106405 (2011).

[25] V. I. Anisimov, A. S. Belozerov, A. I. Poteryaev, and I. Leonov, Phys. Rev. B **86**, 035152 (2012).

[26] A. S. Belozerov, I. Leonov, and V. I. Anisimov, Phys. Rev. B **87**, 125138 (2013).

[27] L. V. Pourovskii, J. Mravlje, A. Georges, S. I. Simak, and I. A. Abrikosov, New J. Phys. **19**, 073022 (2017).

[28] I. Leonov, Phys. Rev. B **92**, 085142 (2015).

[29] I. Leonov, L. Pourovskii, A. Georges, and I. A. Abrikosov, Phys. Rev. B **94**, 155135 (2016).

[30] I. Leonov, A. O. Shorikov, V. I. Anisimov, and I. A. Abrikosov, Phys. Rev. B **101**, 245144 (2020).

[31] E. Greenberg, I. Leonov, S. Layek, Z. Konopkova, M. P. Pasternak, L. Dubrovinsky, R. Jeanloz, I. A. Abrikosov, and G. K. Rozenberg, Phys. Rev. X **8**, 031059 (2018).

[32] P. Villar Arribi and L. de' Medici, Phys. Rev. Lett. **121**, 197001 (2018).

[33] L. de' Medici, Phys. Rev. Lett. **118**, 167003 (2017).

[34] I. Leonov, S. L. Skornyakov, V. I. Anisimov, and D. Vollhardt, Phys. Rev. Lett. **115**, 106402 (2015).

[35] O. Parcollet, M. Ferrero, T. Ayral, H. Hafermann, I. Krivenko, L. Messio, and P. Seth, Comput. Phys. Commun. **196**, 398 (2015).

[36] P. Blaha, K. Schwarz, G. K. H. Madsen, D. Kvasnicka, J. Luitz, R. Laskowski, F. Tran, and L. D. Marks, WIEN2k, An Augmented Plane Wave + Local Orbitals Program for Calculating Crystal Properties (2018).

[37] P. Blaha, K. Schwarz, F. Tran, R. Laskowski, G. K. H. Madsen, and L. D. Marks, J. Chem. Phys. **152**, 074101 (2020).

[38] M. Aichhorn, L. Pourovskii, and A. Georges, Phys. Rev. B **84**, 054529 (2011).

[39] M. Aichhorn, L. Pourovskii, P. Seth, V. Vildosola, M. Zingl, O. E. Peil, X. Deng, J. Mravlje, G. J. Kraberger, C. Martins, M. Ferrero, and O. Parcollet, Comput. Phys. Commun. **204**, 200 (2016).

[40] V. I. Anisimov, D. E. Kondakov, A. V. Kozhevnikov, I. A. Nekrasov, Z. V. Pchelkina, J. W. Allen, S.-K. Mo, H.-D. Kim, P. Metcalf, S. Suga, A. Sekiyama, G. Keller, I. Leonov, X. Ren, and D. Vollhardt, Phys. Rev. B **71**, 125119 (2005).

[41] G. Trimarchi, I. Leonov, N. Binggeli, D. Korotin, and V. I. Anisimov, J. Phys.: Condens. Matter **20**, 135227 (2008).

[42] P. Werner, A. Comanac, L. de' Medici, M. Troyer, and A. J. Millis, Phys. Rev. Lett. **97**, 076405 (2006).

[43] P. Werner and A. J. Millis, Phys. Rev. B **74**, 155107 (2006).

[44] E. Gull, Ph.D. thesis, ETH Zurich, 2008.

[45] L. Boehnke, H. Hafermann, M. Ferrero, F. Lechermann, and O. Parcollet, Phys. Rev. B **84**, 075145 (2011).

[46] L. V. Boehnke, Ph.D. thesis, Universität Hamburg, 2015.

[47] E. Gull, A. J. Millis, A. I. Lichtenstein, A. N. Rubtsov, M. Troyer, and P. Werner, Rev. Mod. Phys. **83**, 349 (2011).

[48] P. Seth, I. Krivenko, M. Ferrero, and O. Parcollet, Comput. Phys. Commun. **200**, 274 (2016).

[49] P. Giannozzi, S. Baroni, N. Bonini, M. Calandra, R. Car, C. Cavazzoni, D. Ceresoli, G. L. Chiarotti, M. Cococcioni, I. Dabo, A. D. Corso, S. de Gironcoli, S. Fabris, G. Fratesi, R. Gebauer, U. Gerstmann, C. Gougoussis, A. Kokalj, M. Lazzeri, L. Martin-Samos *et al.*, J. Phys.: Condens. Matter **21**, 395502 (2009).

[50] T. Miyake and F. Aryasetiawan, Phys. Rev. B **77**, 085122 (2008).

[51] J. Kuneš, A. V. Lukoyanov, V. I. Anisimov, R. T. Scalettar, and W. E. Pickett, Nat. Mater. **7**, 198 (2008).

[52] J. M. Tomczak, T. Miyake, and F. Aryasetiawan, Phys. Rev. B **81**, 115116 (2010).

[53] L. Vaugier, H. Jiang, and S. Biermann, Phys. Rev. B **86**, 165105 (2012).

[54] F. Petocchi, F. Nilsson, F. Aryasetiawan, and P. Werner, Phys. Rev. Research **2**, 013191 (2020).

[55] G. J. Kraberger, R. Triebl, M. Zingl, and M. Aichhorn, Phys. Rev. B **96**, 155128 (2017).

[56] P. E. Blöchl, Phys. Rev. B **50**, 17953 (1994).

[57] G. Kresse and J. Furthmüller, Phys. Rev. B **54**, 11169 (1996).

[58] G. Kresse and J. Furthmüller, Comput. Mater. Sci. **6**, 15 (1996).

[59] A. Zunger, S. H. Wei, L. G. Ferreira, and J. E. Bernard, Phys. Rev. Lett. **65**, 353 (1990).

[60] B. Alling, T. Marten, and I. A. Abrikosov, Phys. Rev. B **82**, 184430 (2010).

[61] J. M. Cowley, Phys. Rev. **77**, 669 (1950).

[62] S. Mandal, K. Haule, K. M. Rabe, and D. Vanderbilt, Phys. Rev. B **100**, 245109 (2019).

[63] S. L. Skornyakov, V. I. Anisimov, and I. Leonov, Phys. Rev. B **103**, 155115 (2021).

[64] A. Charnukha, Z. P. Yin, Y. Song, C. D. Cao, P. Dai, K. Haule, G. Kotliar, and D. N. Basov, Phys. Rev. B **96**, 195121 (2017).

[65] S. L. Skornyakov, V. I. Anisimov, D. Vollhardt, and I. Leonov, Phys. Rev. B **97**, 115165 (2018).

[66] S. L. Skornyakov, V. I. Anisimov, D. Vollhardt, and I. Leonov, Phys. Rev. B **96**, 035137 (2017).

[67] L. de' Medici, Phys. Rev. B **83**, 205112 (2011).

[68] L. de' Medici, J. Mravlje, and A. Georges, Phys. Rev. Lett. **107**, 256401 (2011).

[69] J. Steinbauer, L. de' Medici, and S. Biermann, Phys. Rev. B **100**, 085104 (2019).

[70] A. Isidori, M. Berović, L. Fanfarillo, L. de' Medici, M. Fabrizio, and M. Capone, Phys. Rev. Lett. **122**, 186401 (2019).

[71] A. Georges, L. de' Medici, and J. Mravlje, Annu. Rev. Condens. Matter Phys. **4**, 137 (2013).

[72] K. M. Stadler, G. Kotliar, A. Weichselbaum, and J. von Delft, Ann. Phys. **405**, 365 (2019).

[73] Z. P. Yin, K. Haule, and G. Kotliar, Nat. Mater. **10**, 932 (2011).

[74] X. Deng, K. M. Stadler, K. Haule, A. Weichselbaum, J. von Delft, and G. Kotliar, Nat. Commun. **10**, 2721 (2019).

[75] A. A. Katanin, Nat. Commun. **12**, 1433 (2021).

[76] K. Haule and G. Kotliar, New J. Phys. **11**, 025021 (2009).

[77] S. Mandal, K. Haule, K. Rabe, and D. Vanderbilt, npj Comput. Mater. **5**, 115 (2019).

[78] P. James, O. Eriksson, B. Johansson, and I. A. Abrikosov, Phys. Rev. B **59**, 419 (1999).

[79] I. Leonov, V. I. Anisimov, and D. Vollhardt, Phys. Rev. Lett. **112**, 146401 (2014).

[80] E. Koemets, I. Leonov, M. Bykov, E. Bykova, S. Chariton, G. Aprilis, T. Fedotenko, S. Clément, J. Rouquette, J. Haines, V. Cerantola, K. Glazyrin, C. McCammon, V. B. Prakapenka, M. Hanfland, H.-P. Liermann, V. Svitlyk, R. Torchio, A. D. Rosa, T. Irifune *et al.*, Phys. Rev. Lett. **126**, 106001 (2021).

[81] K. Haule and G. L. Pascut, Phys. Rev. B **94**, 195146 (2016).

[82] K. Haule, J. Phys. Soc. Jpn. **87**, 041005 (2018).

[83] S. Mandal, P. Zhang, S. Ismail-Beigi, and K. Haule, Phys. Rev. Lett. **119**, 067004 (2017).